

Parameter estimation of gravitational wave echoes from exotic compact objects

Andrea Maselli,^{1,*} Sebastian H. Völkel,^{1,†} and Kostas D. Kokkotas¹

¹*Theoretical Astrophysics, Eberhard Karls University of Tuebingen, Tuebingen 72076, Germany*
(Dated: April 15, 2026)

Relativistic ultracompact objects without an event horizon may be able to form in nature and merge as binary systems, mimicking the coalescence of ordinary black holes. The postmerger phase of such processes presents characteristic signatures, which appear as repeated pulses within the emitted gravitational waveform, i.e., echoes with variable amplitudes and frequencies. Future detections of these signals can shed new light on the existence of horizonless geometries and provide new information on the nature of gravity in a genuine strong-field regime. In this work we analyze phenomenological templates used to characterize echolike structures produced by exotic compact objects, and we investigate for the first time the ability of current and future interferometers to constrain their parameters. Using different models with an increasing level of accuracy, we determine the features that can be measured with the largest precision, and we span the parameter space to find the most favorable configurations to be detected. Our analysis shows that current detectors may already be able to extract all the parameters of the echoes with good accuracy, and that multiple interferometers can measure frequencies and damping factors of the signals at the level of percent.

PACS numbers: 04.30.Db, 04.40.Dg, 04.80.Cc, 04.70.Dy

I. INTRODUCTION

Gravitational wave (GW) astronomy is nowadays emerging as a new observational window, able to provide fundamental insights on some of the most energetic phenomena of our Universe. The amount of incoming data produced by ground based interferometers also promises to address questions of fundamental physics with unprecedented accuracy. Among all the possible compact sources, black holes (BH) are probably the most extreme physical systems, whose existence has been definitively assessed by the recent LIGO discoveries [1–3]. These detections mark the dawn of BH spectroscopy and at the same time represent the first genuine strong-field tests of general relativity [4].

However, some crucial questions regarding the fundamental nature of BHs still remain to be addressed [5]. As an example, theoretical models predicting the existence of exotic compact objects (ECOs) whose compactness approaches the BH limit have not been completely ruled out. Such bodies may form in nature as binary systems and merge due to GW emission. During the coalescence the ECOs leave distinct signatures within the inspiral part of the signal, which has already proved to be extremely effective in discriminating between regular BHs and exotic scenarios [6, 7].

After the merger, horizonless compact objects will emit gravitational radiation until they reach a quiet and stationary state. During this process, multiple *trapped w modes* may be excited, which would be visible within the GW signal by the appearance of echolike structures, i.e., repeated pulses with characteristic frequencies and am-

plitudes, which differ from the BH quasinormal modes (QNM) spectrum [8–11].

Historically, the idea that QNM may represent a powerful tool to distinguish between ultracompact stars and regular BHs (or less compact bodies) traces back its origin in some seminal works of the early 1990s [12–17]. A revised application of this approach has recently been applied to interpret the LIGO data in terms of new physics at the level of the BH horizon. This work has drawn a lot of attention [18, 19] and triggered new exciting research efforts in the field [20–27] (see also [28, 29] for some criticism on the same topic). Future detections with a higher signal-to-noise ratio, and the final completion of multiple GW detectors, like VIRGO [30] and KAGRA [31], will provide more accurate data, possibly leading to assess whether horizonless compact bodies may exist in astrophysical environments [32–35].

Several efforts have already been devoted to characterize the GW emission of exotic objects out of equilibrium [18, 36–40]. If additional structures appear within the spectrum, our ability to extract the signatures which deviates from the standard BH picture, will strongly depend on the availability of realistic templates to be used in data searches. In this sense, the recent works by [41, 42] provide the first systematic attempts to construct fully reliable templates to identify the echoes.

Motivated by these results, in this paper we explore for the first time the detectability of GW signals emitted by ECOs formed after binary coalescences. We consider different phenomenological templates, which are physically motivated by the analysis of perturbed ultracompact stars and from a series of recent work on the subject [18, 36–38, 40–42]. The scope of this study is twofold: (i) determine the errors on the waveform’s parameters, which would be measured by current and future GW interferometers, and (ii) investigate the dependence of such detections by the echo’s parameters. Although the mod-

* andrea.maselli@uni-tuebingen.de

† sebastian.voelkel@uni-tuebingen.de

els employed suffer from some limitations, a complete and fully accurate description of the GW signal is nowadays not available. Nevertheless, the analysis developed in this work captures important features of the overall phenomena. Our results suggest that Advanced LIGO at design sensitivity would already be able to constrain the parameters of the echoes with good accuracy, possibly leading to infer new information on the nature of the perturbed compact object.

This paper is organized as follows. In Sec. II we define the analytical templates used to model the echoes, which will be used to determine the parameters' detectability. In Sec. III we briefly describe the data-analysis procedure employed, while in Sec. IV we present our numerical results, analyzing the errors on the gravitational waveforms for different interferometers. In Sec. V we summarize our conclusions. Throughout the paper we will use geometrical units ($G = c = 1$).

II. THE ECHO TEMPLATES

In this section we shall describe the GW templates used to estimate the errors on the echo's parameters. It is worth mentioning that some efforts have recently been made in [18, 41, 42] to propose analytical models that characterize the late time waveform of perturbed exotic objects. In this direction, the main purpose of our paper is to investigate how pure phenomenological waveforms may constrain the fundamental features of the pulses produced after the merger by ultracompact objects with a reflecting surface. We develop our analysis in a pedagogical way, starting from the simplest model, up to more sophisticated waveforms that may eventually mimic the *true* GW emission by a real ECO. For more details on the physics of the echolike structure we refer the reader to the literature that is mentioned in the Introduction. All our models are described by an early ringdown, which represents the fundamental BH QNM damped oscillation, followed by a series of repeated echoes. Hereafter we consider three different templates, defined as follows:

- **echoI**: the waveform is given analytically by $h_I(t) = h_{\text{QNM}}(t) + h_I(t)$, where

$$h_{\text{QNM}}(t) = \bar{\mathcal{A}}e^{-t/\bar{\tau}} \cos(2\pi\bar{f}t + \bar{\phi}), \quad (1)$$

corresponds to the BH QNM-like oscillation, specified by amplitude, frequency, phase, and damping time ($\bar{\mathcal{A}}, \bar{f}, \bar{\phi}, \bar{\tau}$), while

$$h_I(t) = \sum_{n=0}^{N-1} (-1)^{n+1} \mathcal{A}_{n+1} e^{-\frac{y_n^2}{2\beta_1^2}} \cos(2\pi f_1 y_n), \quad (2)$$

describes the N echoes after the first mode. Note that in this case we assume the same frequency and shape (f_1, β_1) for each pulse, but different values of the amplitude $\mathcal{A}_{n+1} = \mathcal{A}_{1,\dots,N}$. For the sake of simplicity we have chosen the modulating function as

a Gaussian profile, with variance given by β_1 . This setup is also in agreement with the analysis developed in [8] to investigate GW signals produced by ultracompact stars perturbed by Gaussian pulses. In the former equation we have also introduced the auxiliary variable $y_n(t) = (t - t_{\text{echo}} - n\Delta t)$, where t_{echo} is the time shift between the first mode and the first echo, while Δt identifies the time delay between the successive $N - 1$ echoes (see Fig. 1).

- **echoIIa**: the first oscillation corresponds again to the BH ringdown mode as in **echoI**, although the echo sector is improved by introducing a second frequency f_2 . The latter takes into account that the frequencies of the pulses we observe in the spectrum are related to the trapped modes of the system, which consist in general of multiple components. The template is then given by

$$h_{\text{II}} = h_{\text{QNM}}(t) + h_{\text{IIa}}(t, f_1, f_2, \beta_1), \quad (3)$$

where

$$h_{\text{IIa}}(t) = \frac{1}{2} \sum_{n=0}^{N-1} (-1)^{n+1} \mathcal{A}_{n+1} e^{-\frac{y_n^2}{2\beta_1^2}} [\cos(2\pi f_1 y_n) + \cos(2\pi f_2 y_n + \phi)], \quad (4)$$

and the phase ϕ determines an offset between the two terms for $t = 0$. Equation (4) describes a beat-like structure, which should mimic as a first approximation the interference of the trapped modes.

- **echoIIb**: this further generalizes the previous approaches by adding a different Gaussian function for the second mode of the echoes, i.e., $h_{\text{II}} = h_{\text{QNM}}(t) + h_{\text{IIb}}(t, f_1, f_2, \beta_1, \beta_2)$, with

$$h_{\text{IIb}}(t) = \frac{1}{2} \sum_{n=0}^{N-1} (-1)^{n+1} \mathcal{A}_{n+1} [e^{-\frac{y_n^2}{2\beta_1^2}} \cos(2\pi f_1 y_n) + e^{-\frac{y_n^2}{2\beta_2^2}} \cos(2\pi f_2 y_n + \phi)]. \quad (5)$$

For all the waveforms we will further assume that amplitudes $\mathcal{A}_{1\dots N}$ carry a fraction of the QNM component $\bar{\mathcal{A}}$. This choice is physically motivated by numerical results obtained from an updated version of a code for ultracompact constant density stars presented in [8], in which the ratio between the QNM mode and the first pulse is roughly equal to $\bar{\mathcal{A}}/\mathcal{A}_1 \sim 1/4$, and then decreases as $\bar{\mathcal{A}}/\mathcal{A}_N \sim \frac{1}{4+N}$ for the following N echoes. This assumption also reduces the number of independent amplitudes to the overall BH-like factor $\bar{\mathcal{A}}$.

The generalization of the previous templates to more sophisticated models is straightforward and could include the following features: (i) add different frequencies and their interference to characterize each echo; (ii) include the damping factor of each frequency (although we expect they would play a subordinate role within the data

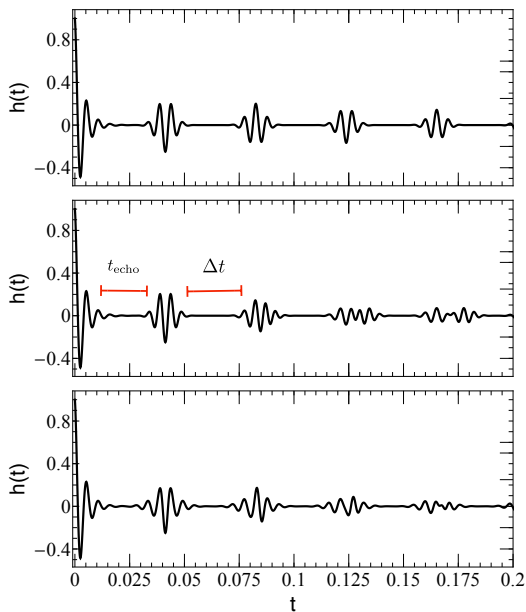


FIG. 1. Sketch of some phenomenological waveforms used in this work. The center panel also shows the meaning of the two parameters t_{echo} and Δt , which identify the time shift between different pulses in the template.

analysis of the waveform); and (iii) introduce different functions to model the shape of the echoes, instead of the Gaussian profile used in this paper. Such improvements would lead one to consider a more realistic scenario, which would ultimately depend on the nature of the ECO's perturbation. These extensions will provide a more detailed picture of the physical mechanism producing the echoes and are under investigation. However, we believe that the GW templates presented in this section are already able to capture the most relevant features of the real process.

III. DATA ANALYSIS PROCEDURE

To compute the errors on the parameters of the echo's template, we use a Fisher matrix approach [43–45]. In the limit of a large signal-to-noise ratio (SNR), the probability distribution of the parameters $\vec{\theta}$ for a given set of data d can be expanded around the true values $\vec{\theta}_v$ as

$$p(\vec{\theta}|d) = p_0(\vec{\theta})\mathcal{L}(d|\vec{\theta}) = p_0(\vec{\theta})e^{-\frac{1}{2}(\vec{h}(\vec{\theta})-d|\vec{h}(\vec{\theta})-d)} \approx p_0(\vec{\theta})e^{-\frac{1}{2}\Gamma_{\alpha\beta}\Delta\theta^\alpha\Delta\theta^\beta}, \quad (6)$$

with $p_0(\vec{\theta})$ being the prior probability on $\vec{\theta}$, and $\Delta\theta^\alpha = \theta^\alpha - \theta_v^\alpha$. The Fisher information matrix $\Gamma_{\alpha\beta}$, which characterizes the curvature of the likelihood function $\mathcal{L}(d|\vec{\theta})$, is expressed in terms of the partial derivatives of the GW

template with respect to the echo parameters,

$$\Gamma_{\alpha\beta} = \left(\frac{\partial \tilde{h}}{\partial \theta^\alpha} \middle| \frac{\partial \tilde{h}}{\partial \theta^\beta} \right)_{\vec{\theta}=\vec{\theta}_v}, \quad (7)$$

where $(\tilde{a}|\tilde{c})$ defines the scalar product on the waveform's space,

$$(\tilde{a}|\tilde{c}) = 2 \int_0^\infty \frac{\tilde{a}(f)\tilde{c}^*(f) + \tilde{a}^*(f)\tilde{c}(f)}{S_n(f)} df, \quad (8)$$

$S_n(f)$ is the noise spectral density of the chosen detector, and $\tilde{h}(f)$ is the Fourier transform of the template in the frequency domain¹. The covariance matrix of the parameters is simply given by the inverse of the Fisher, i.e., $\Sigma_{\alpha\beta} = (\Gamma_{\alpha\beta})^{-1}$, whose diagonal and off-diagonal components correspond to the standard deviations and the correlation coefficients of $\vec{\theta}$, respectively. Note that, according to the Cramer-Rao bound, the uncertainties obtained through the Fisher matrix represent a lower constraint on the variance of any unbiased estimator of the parameters. The scalar product (8) also allows one to define the SNR of the specific signal, as

$$\rho^2 = (\tilde{h}|\tilde{h}) = 4 \int_0^\infty \frac{|\tilde{h}(f)|^2}{S_n(f)} df. \quad (9)$$

In this paper we consider the detectability of echoes by current and future generations of detectors, i.e., Advanced LIGO with the ZERO_DET_highP anticipated design sensitivity curve [46], the Einstein Telescope (ET) [47], LIGO-Voyager (VY) [48], Advanced LIGO with squeezing (LIGO A+) [49], and the Cosmic Explorer (CE) with a wide-band configuration [50]. In the following section we will quote our results on the specific parameter of the template θ^α either in terms of the absolute error σ_α or its relative (percentage) value $\epsilon_\alpha = \sigma_\alpha/\theta^\alpha$.

IV. CONSTRAINTS ON THE ECHO'S PARAMETERS

In this section we present the results for the different templates of Sec. II, obtained by numerical integration of Eqs. (7)-(9). For all the models we choose the frequency and the damping factor of the QNM mode, as those of a nonrotating object with the same mass of the final BH formed in the GW150914 event [51], i.e. $M \simeq 65M_\odot$.

¹ We use the following normalization for the Fourier transform of the templates:

$$\tilde{h}(f) = \int_{-\infty}^\infty h(t) dt, \quad h(t) = \frac{1}{2\pi} \int_{-\infty}^\infty \tilde{h}(f) df.$$

All the waveforms considered yield a full analytical form of $\tilde{h}(f)$, which can be easily computed by means of symbolic manipulation softwares like `Mathematica`.

This yields $\bar{f} \simeq 186$ Hz and $\bar{\tau} \sim 3.6 \times 10^{-3}$ s. Moreover, without loss of generality, we fix the phase of $\bar{h}(t)$ to $\bar{\phi} = 0$, and the overall amplitude to a prototype value $\mathcal{A} = 5 \times 10^{-22}$, which roughly corresponds to a SNR of the QNM-like mode only (i.e., neglecting the contribution of the following echoes) of $\rho \sim 8$ with Advanced LIGO. This value is consistent with the best-fit parameters inferred from GW150914, O1 configuration [51]. Note that, since A represents a multiplicative factor of the total signal, our results can immediately be rescaled to any amplitude A_{new} as

$$\Gamma_{\alpha\beta} \rightarrow \frac{\mathcal{A}_{\text{new}}}{5 \times 10^{-22}} \Gamma_{\alpha\beta} \quad \Rightarrow \quad \sigma_{\alpha} \rightarrow \frac{5 \times 10^{-22}}{\mathcal{A}_{\text{new}}} \sigma_{\alpha}, \quad (10)$$

and in the same way for the SNR,

$$\rho \rightarrow \frac{\mathcal{A}_{\text{new}}}{5 \times 10^{-22}} \rho. \quad (11)$$

After the first pulse, repeated echoes are also expected to occur with a time delay Δt , which depends on the features of the exotic object [5], namely

$$\Delta t \sim 4M |\log \delta|, \quad (12)$$

where $\delta \ll 1$ represents the shift of the ECO's effective surface r_0 with respect to a nonrotating BH horizon located at $2M$ in the Schwarzschild coordinates², i.e. $r_0 = 2M(1 + \delta)$. From Eq. (12), we can approximate the potential well where echoes are reflected, with a box-potential specified by the coordinate width

$$x_c \simeq 2M |\log \delta|. \quad (13)$$

Under this assumption, the correspondence between echoes and trapped modes inside the box allows one to express the gap between two consecutive modes Δf with frequencies f_{n+1}^{box} and f_n^{box} as

$$\Delta f \equiv f_{n+1}^{\text{box}} - f_n^{\text{box}} \simeq \frac{1}{4M |\log \delta|}. \quad (14)$$

Then, having fixed the first frequency of each waveform to the corresponding BH QNM component, we can immediately derive the values of f_1 and f_2 used in the **echoI** and **echoIIa-b** templates:

$$f_1 \simeq \bar{f}, \quad f_2 \simeq \bar{f} - \Delta f. \quad (15)$$

² The coordinate distance is not gauge invariant, and therefore in general the specific value of δ is not uniquely defined. However the difference with respect to the proper distance is subordinate in our calculations due to the logarithmic dependence within r_0 . Note also that the approximations for small δ are only valid for systems, where the reflecting surface is very close to the BH horizon in the Schwarzschild coordinate. Although constant density stars can feature a similar structure, the values of δ for such objects can never be small, due to the Buchdahl limit.

Note that $f_2 < f_1$. It is worthwhile to remark that these assumptions represent an approximation of the real physical scenario, in which we expect that $\bar{f} \neq f_1$, and Δf takes a more complex form, which ultimately depends on the specific ECO considered. However, for the purpose of this paper, this will not change the outcome of the data-analysis procedure. Moreover, having fixed the object mass to $M = 65M_{\odot}$, throughout this paper we consider three values of $\delta = (10^{-10}, 10^{-20}, 10^{-30})$, which roughly correspond to compact objects with surface corrections at Micron, Fermi, and Planckian levels, respectively [7].

Finally, the time between the QNM-like mode and the first echo, t_{echo} , could be affected by nonlinearities due to the merger phase at the end of the coalescence [52], i.e., $t_{\text{echo}} \simeq \Delta t \pm \delta t$. In the following, for each value of Δt given by Eq. (12), we will consider different configurations by varying the coefficient δt in order to have a maximum correction of the order 10% on t_{echo} .

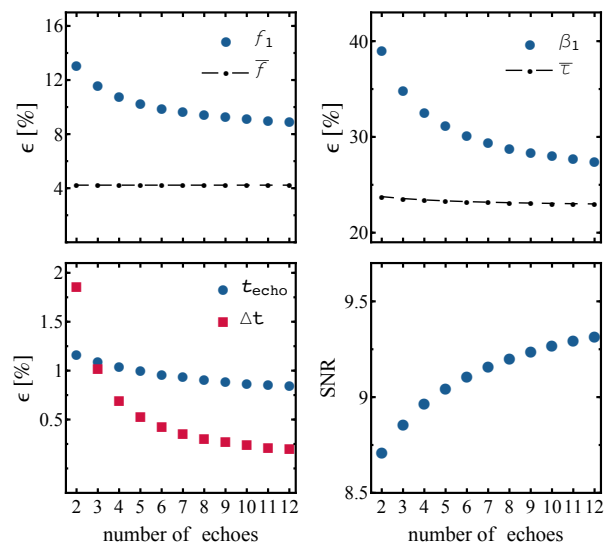


FIG. 2. Relative (percentage) errors on the parameters of the template **echoI** as a function of the number of echoes. All the results are derived for Advance LIGO, assuming $\delta = 10^{-10}$ and $\beta_1 = 0.003$. The bottom right panel shows the change of the signal-to-noise ratio due to the increasing numbers of echoes.

Before assessing the detectability of each phenomenological template described in the previous section, it is instructive to analyze some basic features that are common to all the waveforms. Figure 2 shows the relative errors ϵ_{α} for the **echoI** model computed for LIGO, as a function of the number of echoes included within the template. In this particular case we assume $\beta_1 = 0.003$ and $\delta = 10^{-10}$, which corresponds to $t_{\text{echo}} = \Delta t \simeq 2.95 \times 10^{-2}$ s. From the first two panels we can immediately note that the uncertainty on frequency and damping time of the QNM component (black dots) is essentially unaffected by N ,

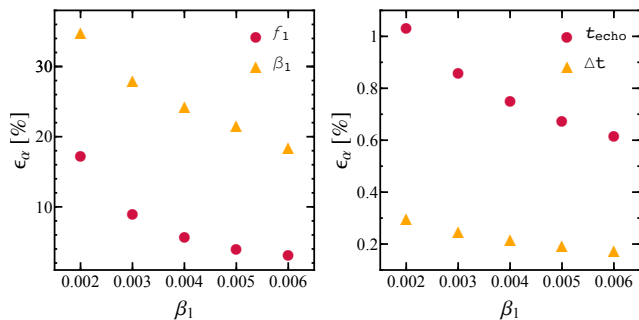


FIG. 3. Relative (percentage) errors on the parameters of the template **echoI** computed for Advanced LIGO, as a function of the width of the Gaussian width β_1 . Both panels refer to $t_{\text{echo}} \approx \Delta t \approx 2.95 \times 10^{-2}$ ($\delta = 10^{-10}$).

and it is therefore independent³ from the template (2). On the other hand, the errors on (f_1, β_1) and on the delay times $(t_{\text{echo}}, \Delta t)$ reduce as far as the number of pulses grows in time. For the particular model analyzed here, the uncertainty on both f_1 and β_1 changes approximately 30% between $N = 2$ and $N = 10$. Although these values seem to converge to the QNM mode value, this decrease saturates due to the progressive reduction of the echo's amplitudes. This feature is also evident looking at the evolution of the overall SNR (right-bottom panel of Fig. 2), which reaches a nearly constant value of $\rho \sim 9.3$ after 12 pulses. This picture is nearly independent of the range of parameters used in this work and of the specific echo model adopted.

According to these results, we can safely consider gravitational waveforms that include 10 pulses after the QNM oscillation, since larger values of N will not affect the analysis. This choice will also make our analysis more robust, since at later times some physical effects may not be captured by our models (as the interference of multiple trapped frequencies).

A. **echoI**

The simplest waveform **echoI** depends on the following set of parameters: $\vec{\theta} = \{\ln \mathcal{A}, \bar{f}, \bar{\tau}, \bar{\phi}, f_1, \beta_1, t_{\text{echo}}, \Delta t\}$, which lead to an 8×8 Fisher matrix. As described before, we fix the frequency and damping factor of the QNM, with f_1 and the time shift Δt being specified by Eqs. (12) and (15). However, to explore the space of the parameter's configurations, we vary the shape factor β_1 and $t_{\text{echo}} = \Delta t + \delta t$. This will allow one to determine the more (or less) favorable signals to be detected by GW interferometers. The width of the echo's Gaussian function represents the coefficient that dominantly affects the shape

of the waveform and therefore leads to major changes in the parameter estimation. Moreover, we will only discuss the features of the post-QNM modes, since the errors on \bar{f} and $\bar{\tau}$ do not vary significantly within all the configurations, peaking around $\epsilon_{\bar{f}} \sim 4\%$ and $\epsilon_{\bar{\tau}} \sim 22\%$ - 23% , respectively.

Figure 3 shows the uncertainties of the **echoI** parameters as a function of β_1 computed for Advanced LIGO, for a specific configuration with $t_{\text{echo}} \approx \Delta t$ and $\delta = 10^{-10}$. We immediately see from both panels that all relative errors rapidly decrease as the shape factor grows, with variations $\gtrsim 40\%$ for ϵ_{f_1} and ϵ_{β_1} . Note that the SNR changes between $\rho \sim 8.9$ for $\beta_1 = 0.002$ to $\rho \sim 10.3$ for $\beta_1 \sim 0.006$ with an overall increase of 15%. It is important to remark that, although these differences do exist between the various configurations, all the modes considered yield errors smaller than a $1\text{-}\sigma$ upper bound with $\epsilon_{\alpha} = 1$. This is particularly promising for the measurements of the time shift parameters (right panel), which can be constrained with an accuracy better than 1%.

The dependence of σ_{α} with respect to t_{echo} [which we vary in our data set as $t_{\text{echo}} = \Delta t(1 \pm 0.1)$] is much milder and leads to nearly constant errors for all the parameters of the template. This can be appreciated from the contour plots of Fig. 4, in which curves of fixed accuracy for f_1, β_1 , and Δt are given by vertical straight lines. Note that the *relative* errors on t_{echo} (bottom left) change less than 10% within the parameter space considered, even though the *absolute* error remains practically constant.

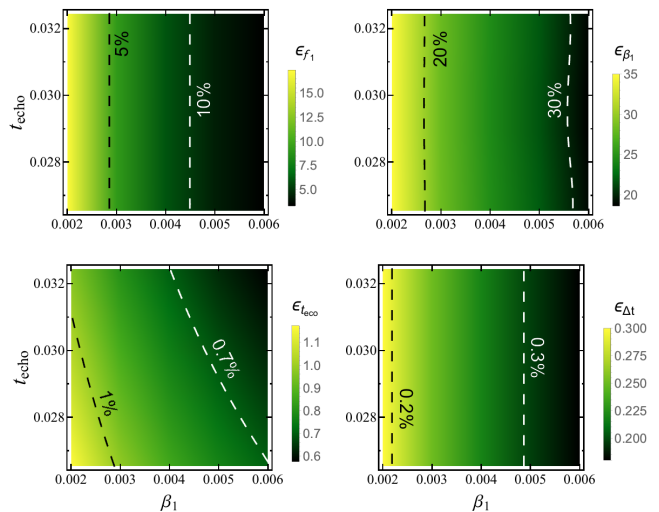


FIG. 4. Contour plots in the $\beta_1 - t_{\text{echo}}$ parameter space for the relative errors on the **echoI** parameters. White and black dashed curves represent configurations with fixed accuracy. The data refer to Advanced LIGO at design sensitivity.

Although Advanced LIGO (at design sensitivity) seems already able to set narrow bounds on some of the echo's features, it is interesting to investigate how these results improve as far as we consider next generation detectors. This is shown in Fig. 5, in which we draw the relative er-

³ The correlation coefficients derived from the Fisher matrix between \bar{f} ($\bar{\tau}$) and the echo parameters are also very small for all the configurations.

rors of **echoI** for different interferometers. All the results correspond to the best-case scenario, i.e., for $\beta_1 = 0.006$. Note also that in general, for fixed β_1 , the best measurements for each detector will correspond to a different value of t_{echo} (although changing this variable does not yield significant variations). Looking at the top panel we note that the errors of the echo's shape factor decrease to values of the order of $\leq 1\%$ already with LIGO A+, while for the frequency f_1 , the same level of accuracy would require at least the ET. As expected, the recently proposed CE would lead to detect GW signals with exquisite precision, with errors being more than an order of magnitude smaller than values obtained by the current generation of detectors.

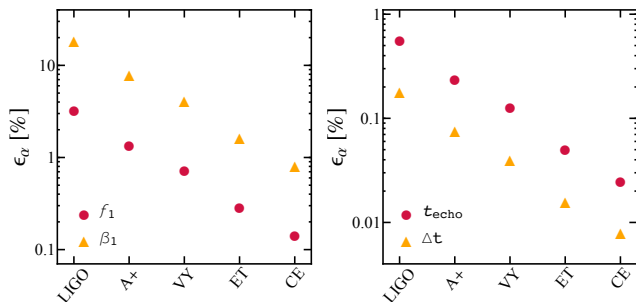


FIG. 5. Errors on the **echoI** template for different GW interferometers. The data refer to the best case scenario with $\beta_1 = 0.006$ (and different values of t_{echo}).

Second generation interferometers are also expected to form a network of ground based detectors, as soon as Advanced Virgo and KAGRA join the Hanford and Livingston LIGO sites. A collection of n independent interferometers will roughly reduce the error by a coefficient $1/\sqrt{n}$. Looking at Fig. 5 this factor would translate the network measurements at the same level of LIGO A+.

All the results presented so far are derived assuming a shift of the ECO's effective surface equal to $\delta = 10^{-10}$, which (together with the mass) determines the two time-delay factors of our template. To test alternative scenarios, we have considered different configurations by varying δ to 10^{-20} and 10^{-30} , without finding significant deviations from the data shown in Figs. 3-5. The parameters being mostly affected, f_1 and β_1 , lead to changes $\lesssim 9\%$ and $\lesssim 2\%$, respectively, while for the other coefficients we observe variations below 1% . The values of $\epsilon_{t_{\text{echo}}}$ and $\epsilon_{\Delta t}$ do actually change, although the corresponding absolute errors remain constant. This means that the uncertainties for the new values of δ can simply be obtained from the previous results, by rescaling

$$\epsilon_{t_{\text{echo}}}\Big|_{\delta=10^{-20}} = \epsilon_{t_{\text{echo}}}\Big|_{\delta=10^{-10}} \frac{t_{\text{echo}}(\delta = 10^{-10})}{t_{\text{echo}}(\delta = 10^{-20})}, \quad (16)$$

and the same for Δt .

B. **echoIIa-b**

The **echoIIa** model introduces two extra parameters: (i) a second frequency within the spectrum, which leads to a beatlike interference with the first component, and (ii) a phase offset ϕ between the two echo modes. These extra parameters further enlarge the space of configurations to a 10×10 Fisher matrix. This extension does not alter the estimate of \bar{f} and $\bar{\tau}$, whose errors remain unchanged compared to the values obtained for the previous template. Moreover, as already described for **echoI**, all the results are nearly degenerate with respect to t_{echo} , as changes on this parameter do not lead to sensible variations of the errors. For this reason we will only focus on the dependence of the echo's errors on β_1 .

The parameter estimation of this toy model template shows that the results are strongly affected by the choice of ϕ . In particular the error distribution finds a minimum when the echo modes are out of phase with $\phi = -\pi/2$, while it is maximum when the two components are on phase, i.e., $\phi = 0$. This effect is particularly relevant for (f_1, f_2, β_1) , as shown in the left panel of Fig. 6 in which we draw the corresponding relative uncertainties computed for LIGO, assuming $\delta = 10^{-10}$. As already seen for **echoI**, all the errors decrease with the growth of the shape factor, up to our best model with $\beta_1 = 0.006$. The two frequencies yield almost the same accuracy for $\phi = 0$, while for out-of-phase modes the errors on f_2 are in general larger and converge to ϵ_{f_1} for $\beta_1 \gtrsim 0.004$ only. Figure 6 also shows that our ability to measure the width of the Gaussian function strongly depends on the phase of the echoes, as for $\phi = 0$ all of the configurations lead to errors above an upper bound $\epsilon_{\beta_1} = 1$. This picture changes dramatically if $\phi = -\pi/2$, for which the uncertainties on this parameter is of the same order of magnitude as (f_1, f_2) , and smaller than 50% for $\beta_1 > 0.002$. Variations of ϕ are subordinate on t_{echo} and Δt , for which we observe small deviations between the two cases. The center panel of Fig. 6 shows that even for this template the two parameters provide the best measurements, at the level of percent and below.

As expected, even for the most optimistic scenario ($\phi = -\pi/2$), the results obtained for this model are in general worse than those derived for the **echoI** (cf. Fig. 3). This change is partially due to the larger number of parameters which, for a given configuration and detector sensitivity, dilutes the amount of information contained within the waveform. In this regard, it is also interesting to compare how the specific form of the waveform may influence the SNR of the signal (and the degeneracies between the parameters). The right panel of Fig. 6 shows indeed how this quantity changes as a function of β_1 for **echoI** and **echoIIa** (and two values of ϕ). The picture leads to some interesting conclusions. First, we observe that for all cases considered the second parametrization yields lower SNR. Moreover, the overall growth is softer, with an increase of $\sim 9\%$ - 12% (depending on the value of ϕ) compared to a change of

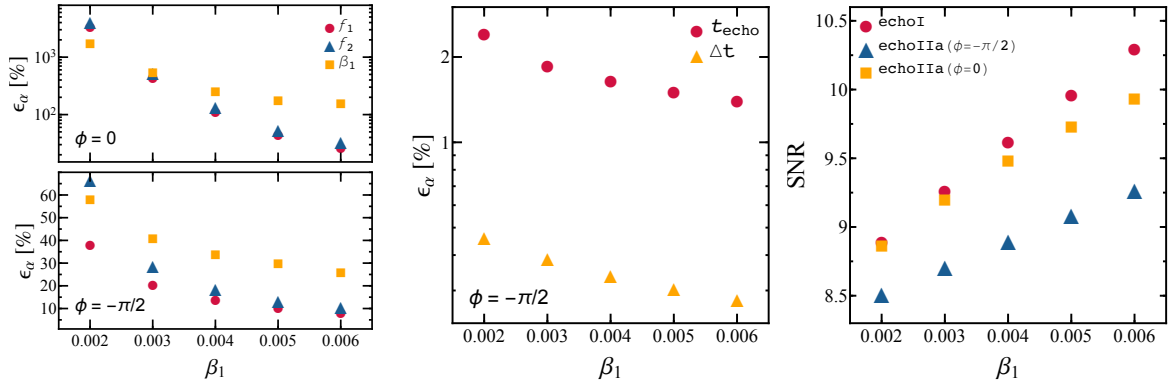


FIG. 6. (Left and center panels) Same as Fig. 3 but for the parameters of the `echoIIa` model with phase shift $\phi = 0$ and $\phi = -\pi/2$. (Right panel) Comparison between the SNR of `echoI` and `echoIIa` as a function of β_1 . All the results refer to Advanced LIGO, assuming $t_{\text{echo}} \approx \Delta t$, with $\delta = 10^{-10}$.

$\sim 16\%$ for the first template. More significantly, the values of ρ for $\phi = -\pi/2$ are always smaller than those for $\phi = 0$, which is a rather counterintuitive result, as the errors scale in the opposite direction. In this case a major role is played by the degeneracy between the parameters, as shown in Fig. 7 where the correlation coefficients $c_{\alpha\beta} = \Sigma_{\alpha\beta}/(\sigma_\alpha\sigma_\beta)$ between f_1 and (β_1, f_2) are plotted. For $\phi = 0$ the two components of the echoes (4) are described exactly by the same functional form, and all the variables are extremely correlated, as for the two frequencies for which $c_{f_1 f_2} \simeq -1$. Note that in the limit $f_1 \rightarrow f_2$ we would have 100% degeneracy. Conversely, for out-of-phase modes with $\phi = -\pi/2$ we have a maximum break of such degeneracy that allows one to set tighter constraints on the parameters. Moreover, the values of $c_{f_1 \beta}$ for $\beta = \{t_{\text{echo}}, \Delta t\}$ are always close to zero for any choice of ϕ , which is in line with the results previously described.

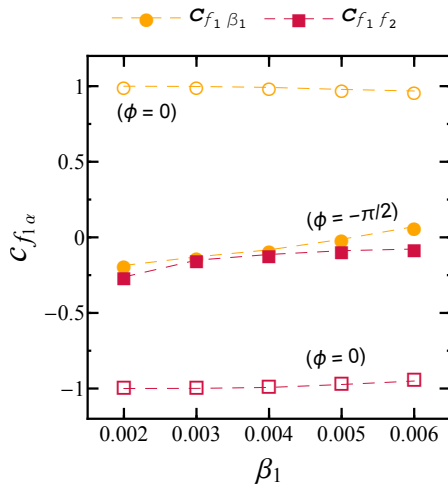


FIG. 7. Correlation coefficients for the `echoIIa` template between f_1 and (β_1, f_2) , assuming $\phi = 0$ (empty dots) and $\phi = -\pi/2$ (empty dots), for LIGO with $\delta = 10^{-10}$ and $t_{\text{echo}} \approx \Delta t$.

Finally, unlike the `echoI`, the second template is more sensible to different values of δ . Comparing the results obtained for $\delta = 10^{-30}$ and $\delta = 10^{-10}$, assuming the optimal case $\beta_1 = 0.006$ and $\phi = -\pi/2$, we find that the absolute errors of $\{f_1, \beta_1, f_2, t_{\text{echo}}, \Delta t\}$ vary approximately as $\simeq \{23, -12, -8, -6, -41\}\%$, and therefore a scaling such as that given by Eq. (16) is no longer valid. These differences grow dramatically for $\phi = 0$.

As the last step we analyze the output of the `echoIIb` model, which improves the former description by adding another shape factor (β_2) to the second component of the pulses, specified by the frequency f_2 . For the sake of simplicity, in this case we will fix $\delta = 10^{-10}$ and $t_{\text{echo}} = \Delta t$. Then, we span the possible configurations within the $\beta_1 \times \beta_2$ parameter space, also assuming the two phase shifts considered before, i.e., $\phi = 0$ and $\phi = -\pi/2$. Figure 8 shows the numerical results obtained for the latter, assuming the LIGO detector.

From the top panels we observe that the relative errors on (f_1, β_1) are nearly degenerate with respect to the Gaussian width of the second component. The opposite occurs if we look at the behavior of ϵ_{f_2} and ϵ_{β_2} in the bottom plots. This feature is mainly due to the specific form of the template, such that the diagonal components of the Fisher matrix for the first mode is independent of the second one and vice versa. In both cases, however, a sweet spot exists for larger values of the shape factors that yield the best results. This clearly confirms the trend observed for the `echoI` and `echoIIa` templates. Note also that the parameter's accuracy of both modes is comparable. Only a few configurations, clustered around $\beta_2 \simeq 0.002$, lead to errors on f_2 and β_2 exceeding the upper bound $\epsilon_\alpha = 1$. The relative uncertainties on the time shifts (not shown in the figure) are in agreement with the results obtained for the previous waveforms, with $\epsilon_{\text{echo}} \lesssim 3\%$ and $\Delta t \lesssim 1\%$ for all the points in the $\beta_1 \times \beta_2$ plane.

A phase shift $\phi = 0$ between the echo's components would, again, reduce our ability to detect frequencies and shape factors. This is shown in Fig. 9, in which each point

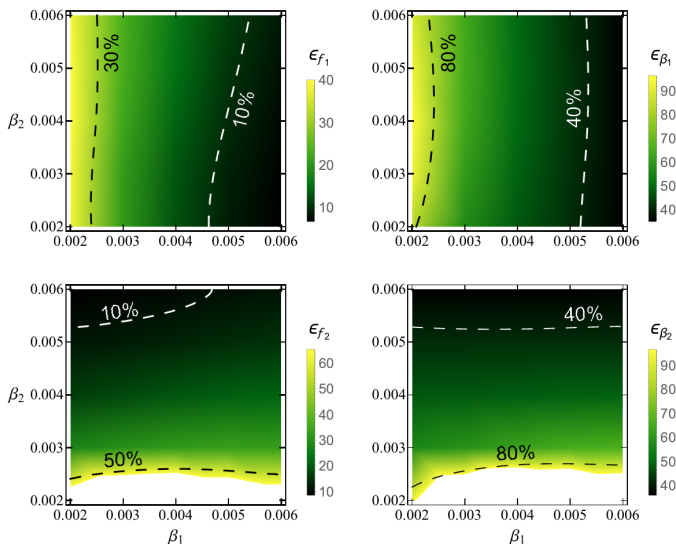


FIG. 8. Same as Fig. 4 but for the parameters of `echoIIB` in the $\beta_1 \times \beta_2$ plane. The phase offset is fixed to $\phi = -\pi/2$.

identifies a specific configuration for which the relative error of a certain parameter is larger than 1, i.e., for which its measurement is strictly compatible with zero.

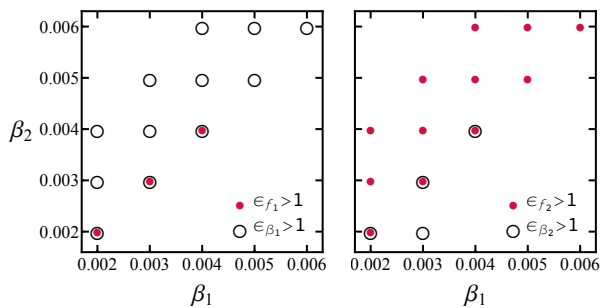


FIG. 9. Each dot specifies a configurations in the $\beta_1 \times \beta_2$ plane with $\phi = 0$ for which the relative error $\epsilon_\alpha > 1$.

This picture rapidly improves for future detectors as demonstrated in Fig. 10, in which we plot the errors corresponding to the best configurations, with $\phi = -\pi/2$. Note that the most accurate results occur when the difference between the two Gaussian widths is maximum, i.e., when $(\beta_1, \beta_2) = (0.006, 0.002)$ for ϵ_{f_1} and ϵ_{β_1} , and when $(\beta_1, \beta_2) = (0.002, 0.006)$ for ϵ_{f_2} and ϵ_{β_2} . The picture shows, for example, that LIGO A+ (which we remind the reader roughly corresponds to a network of current detectors) would already constrain frequencies and shape factors with a relative accuracy around $\ll 10\%$. A third generation detector like the Einstein Telescope would be required to reduce these errors below 1%.

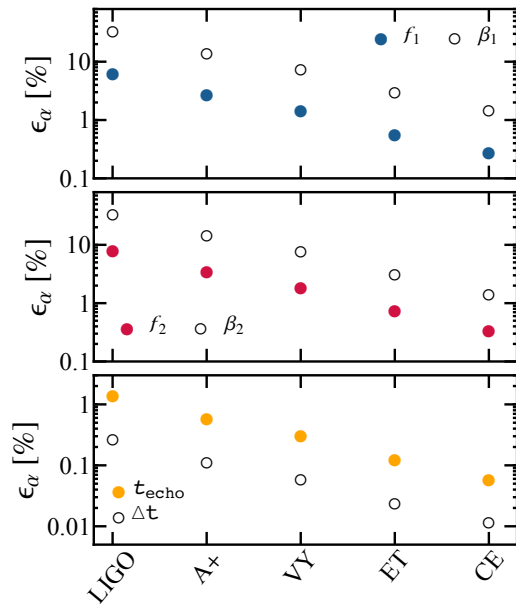


FIG. 10. Relative errors of the `echoIIB` model for the best case scenario with $\phi = -\pi/2$, computed for different interferometers.

V. CONCLUSIONS

Gravitational wave astronomy is establishing itself as a new field of research capable of gaining insights on a genuine strong field gravity regime, and answering open questions of fundamental physics. A key example is given by the possible existence of horizonless exotic objects whose compactness approaches the BH limit. Such ECOs may form in nature and merge within the Hubble time, mimicking the last stage of coalescence of two ordinary BHs [6]. In the postmerger phase, these objects would produce characteristic echoes, which at late time differ from the standard QNM spectrum, and can in principle be detected by laser interferometers. Although current GW data seem to show no statistical evidence of possible deviations from the standard BH picture, it is expected that signals with larger SNR will provide new precious information. For this purpose it is mandatory to construct GW templates as accurately as possible, which allow one to capture the dominant features of the process. Recent efforts have already been done to build fully analytical waveforms for data analysis strategies [41, 42]. In this paper we pursue a complementary path, trying to address for the first time the level of accuracy with which current/near future interferometers will be able to detect the echo's parameters. To this aim we have adopted phenomenological templates depending on a relatively small set of coefficients, which try to mimic the expected *true* signal with an increasing degree of realism.

The numerical results obtained for all the considered models seem to suggest that even current detectors, at design sensitivity, can provide reliable estimates of all

the parameters. Moreover, the analysis performed for the templates highlights some common properties, which can be described as follows:

- The SNR and the errors of realistic echo signals are expected to saturate after a certain number of repeated reflections, as the amplitude of each pulse decreases in time.
- The uncertainties on the template’s parameters are mostly affected by the width of the function that shapes the echoes. In particular, larger values of this factor always lead to an increase of the overall SNR and to a reduction of the errors.
- As far as multiple frequencies are considered, the phase offset between different components of the echoes plays a crucial role, and it strongly affects the degeneracy between the parameters. Modes out of phase (in phase) lead to minimum (maximum) errors.
- Best case scenarios for all the models show that the frequencies and the shape factors of the echoes can always be measured with an accuracy smaller than 100%. A network of advanced detectors, composed of the two LIGO, Virgo and KAGRA, would reduce these values around 10%. Third generation interferometers, such as the Einstein Telescope, are required to measure the same quantities at the level of percent.
- The parameters that characterize the time delay between the BH QNM component and the subsequent echoes are measured with exquisite accuracy, with relative errors $\lesssim 3\%$ with Advanced LIGO already. Moreover changes in t_{echo} and Δt seem to slightly affect the other parameters of the waveform.
- Complex templates, in which multiple frequencies may interfere to produce the echoes, are more sensitive to variations of the parameter δ which controls

the shift between the ECO’s surface with respect to a Schwarzschild BH horizon.

A summary of the results for the most complex model can be found in Figs. 8-10.

The data analysis developed in this paper may be considered as a proof of principle for future developments, and it suffers from two main limitations. The first obvious drawback is given by the lack of a semianalytical template able to fully characterize the GW emission of perturbed ECOs. The phenomenological models used here represent a first step in this direction, which provide a reliable description of the full picture, being still based on a limited numbers of parameters. Note that, unlike standard QNMs, which are solely determined by the BH mass and spin, the echo structure is intrinsically more complex as follows: (i) the trapped modes spectrum crucially depends on the specific ECO considered, and (ii) the shape of the echoes can be affected by the specific form of the perturbation. A second source of uncertainty, connected to the previous problem, relies on the unique identification of the echo’s amplitudes. Although the assumptions employed in Sec. II are physically motivated by well known results [8], our conclusions still depend on the relative strength of the pulses and can be considered as an optimistic scenario.

Improvements of the previous points can pursue various directions. Our current efforts are particularly devoted to investigate in detail the following aspects: (i) construct more refined models that approach realistic ultracompact objects with larger accuracy, possibly taking into account the interference of multiple trapped modes; (ii) use a fully Bayesian analysis to perform model selection and assess the ability of the ground based interferometer to distinguish between standard BH and echolike signals; and (iii) employ realistic errors to reconstruct the ECO’s scattering potential by measurements of the trapped modes, as done in [27]. These extensions are already under investigation.

Acknowledgements.— S.V. is grateful for the financial support of the Baden-Württemberg Foundation.

-
- [1] B. P. Abbott *et al.* (LIGO Scientific Collaboration and Virgo Collaboration), *Phys. Rev. Lett.* **116**, 061102 (2016).
- [2] B. P. Abbott *et al.* (LIGO Scientific Collaboration and Virgo Collaboration), *Phys. Rev. Lett.* **116**, 241103 (2016).
- [3] B. P. Abbott *et al.* (LIGO Scientific and Virgo Collaboration), *Phys. Rev. Lett.* **118**, 221101 (2017).
- [4] B. P. Abbott *et al.* (LIGO Scientific and Virgo Collaborations), *Phys. Rev. Lett.* **116**, 221101 (2016).
- [5] V. Cardoso and P. Pani, (2017), [arXiv:1707.03021 \[gr-qc\]](#).
- [6] V. Cardoso, E. Franzin, A. Maselli, P. Pani, and G. Raposo, *Phys. Rev.* **D95**, 084014 (2017), [Addendum: *Phys. Rev.* **D95**, no.8, 089901 (2017)], [arXiv:1701.01116 \[gr-qc\]](#).
- [7] A. Maselli, P. Pani, V. Cardoso, T. Abdelsalhin, L. Gualtieri, and V. Ferrari, (2017), [arXiv:1703.10612 \[gr-qc\]](#).
- [8] K. D. Kokkotas, in *Relativistic gravitation and gravitational radiation. Proceedings, School of Physics, Les Houches, France, September 26-October 6, 1995* (1995) pp. 89–102, [arXiv:gr-qc/9603024 \[gr-qc\]](#).
- [9] K. Tominaga, M. Saijo, and K.-i. Maeda, *Phys. Rev. D* **60**, 024004 (1999).
- [10] V. Ferrari and K. D. Kokkotas, *Phys. Rev. D* **62**, 107504 (2000), [gr-qc/0008057](#).
- [11] J. Ruoff, *Phys. Rev. D* **63**, 064018 (2001).
- [12] S. Chandrasekhar and V. Ferrari, *Proceedings of the*

- Royal Society of London Series A **434**, 449 (1991).
- [13] S. Chandrasekhar and V. Ferrari, *Proceedings of the Royal Society of London Series A* **432**, 247 (1991).
- [14] K. D. Kokkotas and B. F. Schutz, *Mon. Not. R. Astron. Soc.* **255**, 119 (1992).
- [15] K. D. Kokkotas, *Mon. Not. R. Astron. Soc.* **268**, 1015 (1994).
- [16] Y. Kojima, N. Andersson, and K. D. Kokkotas, *Proceedings of the Royal Society of London Series A* **451**, 341 (1995), [gr-qc/9503012](#).
- [17] N. Andersson, Y. Kojima, and K. D. Kokkotas, *Astrophys. J.* **462**, 855 (1996), [gr-qc/9512048](#).
- [18] J. Abedi, H. Dykaar, and N. Afshordi, ArXiv e-prints (2016), [arXiv:1612.00266 \[gr-qc\]](#).
- [19] J. Abedi, H. Dykaar, and N. Afshordi, ArXiv e-prints (2017), [arXiv:1701.03485 \[gr-qc\]](#).
- [20] C. Barceló, R. Carballo-Rubio, and L. J. Garay, *Journal of High Energy Physics* **2017**, 54 (2017).
- [21] R. Price and G. Khanna, ArXiv e-prints (2017), [arXiv:1702.04833 \[gr-qc\]](#).
- [22] S. H. Völkel and K. D. Kokkotas, *Classical and Quantum Gravity* **34**, 125006 (2017), [arXiv:1703.08156 \[gr-qc\]](#).
- [23] E. Maggio, P. Pani, and V. Ferrari, ArXiv e-prints (2017), [arXiv:1703.03696 \[gr-qc\]](#).
- [24] R. Brustein, A. J. M. Medved, and K. Yagi, ArXiv e-prints (2017), [arXiv:1704.05789 \[gr-qc\]](#).
- [25] S. Hod, ArXiv e-prints (2017), [arXiv:1704.05856 \[hep-th\]](#).
- [26] B. Holdom and J. Ren, *Phys. Rev. D* **95**, 084034 (2017).
- [27] S. H. Völkel and K. D. Kokkotas, *Classical and Quantum Gravity* **34**, 175015 (2017), [arXiv:1704.07517 \[gr-qc\]](#).
- [28] C. Chirenti and L. Rezzolla, *Phys. Rev. D* **94**, 084016 (2016), [arXiv:1602.08759 \[gr-qc\]](#).
- [29] G. Ashton, O. Birnholtz, M. Cabero, C. Capano, T. Dent, B. Krishnan, G. D. Meadors, A. B. Nielsen, A. Nitz, and J. Westerweck, ArXiv e-prints (2016), [arXiv:1612.05625 \[gr-qc\]](#).
- [30] <https://dcc.ligo.org/LIGO-P1200087-v19/public>.
- [31] <http://gwcenter.icrr.u-tokyo.ac.jp/en/researcher/parameter>.
- [32] E. Berti, A. Sesana, E. Barausse, V. Cardoso, and K. Belczynski, *Phys. Rev. Lett.* **117**, 101102 (2016).
- [33] V. Cardoso and L. Gualtieri, *Classical and Quantum Gravity* **33**, 174001 (2016), [arXiv:1607.03133 \[gr-qc\]](#).
- [34] H. Yang, K. Yagi, J. Blackman, L. Lehner, V. Paschalidis, F. Pretorius, and N. Yunes, *Phys. Rev. Lett.* **118**, 161101 (2017).
- [35] A. Maselli, K. D. Kokkotas, and P. Laguna, *Phys. Rev. D* **95**, 104026 (2017).
- [36] T. Damour and S. N. Solodukhin, *Phys. Rev. D* **76**, 024016 (2007), [arXiv:0704.2667 \[gr-qc\]](#).
- [37] C. B. M. H. Chirenti and L. Rezzolla, *Classical and Quantum Gravity* **24**, 4191 (2007), [arXiv:0706.1513 \[gr-qc\]](#).
- [38] V. Cardoso, E. Franzin, and P. Pani, *Physical Review Letters* **116**, 171101 (2016), [arXiv:1602.07309 \[gr-qc\]](#).
- [39] R. A. Konoplya and A. Zhidenko, *JCAP* **1612**, 043 (2016), [arXiv:1606.00517 \[gr-qc\]](#).
- [40] V. Cardoso, S. Hopper, C. F. B. Macedo, C. Palenzuela, and P. Pani, *Phys. Rev. D* **94**, 084031 (2016), [arXiv:1608.08637 \[gr-qc\]](#).
- [41] H. Nakano, N. Sago, H. Tagoshi, and T. Tanaka, (2017), [10.1093/ptep/ptx093](#), [arXiv:1704.07175 \[gr-qc\]](#).
- [42] Z. Mark, A. Zimmerman, S. M. Du, and Y. Chen, ArXiv e-prints (2017), [arXiv:1706.06155 \[gr-qc\]](#).
- [43] A. Królak, J. A. Lobo, and B. J. Meers, *Phys. Rev. D* **48**, 3451 (1993).
- [44] K. Kokkotas, A. Królak, and G. Tsegas, *Classical and Quantum Gravity* **11**, 1901 (1994).
- [45] M. Vallisneri, *Phys. Rev. D* **77**, 042001 (2008), [arXiv:gr-qc/0703086 \[GR-QC\]](#).
- [46] <https://dcc.ligo.org/cgi-bin/DocDB/ShowDocument?docid=2974>.
- [47] S. Hild, S. Chelkowski, A. Freise, J. Franc, N. Morgado, R. Flaminio, and R. DeSalvo, *Class. Quant. Grav.* **27**, 015003 (2010), [arXiv:0906.2655 \[gr-qc\]](#).
- [48] <https://dcc.ligo.org/public/0120/T1500290/002/T1500290.pdf>.
- [49] J. Miller, L. Barsotti, S. Vitale, P. Fritschel, M. Evans, and D. Sigg, *Phys. Rev. D* **91**, 062005 (2015), [arXiv:1410.5882 \[gr-qc\]](#).
- [50] B. P. A. et al., *Classical and Quantum Gravity* **34**, 044001 (2017).
- [51] B. P. Abbott *et al.* (Virgo, LIGO Scientific), *Phys. Rev. Lett.* **116**, 221101 (2016), [arXiv:1602.03841 \[gr-qc\]](#).
- [52] J. Abedi, H. Dykaar, and N. Afshordi, (2016), [arXiv:1612.00266 \[gr-qc\]](#).